Cell
PRESS

Structural Insights into Membrane Interaction and Caveolar Targeting of Dynamin-like EHD2

Claudio Shah,[1,2,8] Balachandra G. Hegde,[3,8] Björn Morén,[4] Elmar Behrmann,[5] Thorsten Mielke,[5,6] Gregor Moenke,[1] Christian M.T. Spahn,[5] Richard Lundmark,[4] Oliver Daumke,[1,2,5,*] and Ralf Langen[7,*]

[1]Max-Delbrück-Center for Molecular Medicine, Crystallography, Robert-Rössle-Straße 10, 13092 Berlin, Germany
[2]Institute of Chemistry and Biochemistry, Freie Universität Berlin, Takustraße 6, 14195 Berlin, Germany
[3]Post Graduate Department of Physics, Rani Channamma University, Vidyasangama, Belagavi-591156, India
[4]Medical Biochemistry and Biophysics, Umeå University, 901 87 Umeå, Sweden
[5]Institute of Medical Physics and Biophysics, Charité, Charitéplatz 1, 10117 Berlin, Germany
[6]UltraStrukturNetzwerk, Max-Planck-Institute for Molecular Genetics, Ihnestraße 73, 14195 Berlin, Germany
[7]Zilkha Neurogenetic Institute, University of Southern California, 1501 San Pablo Street, Los Angeles, CA 90033, USA
[8]These authors contributed equally to this work
*Correspondence: oliver.daumke@mdc-berlin.de (O.D.), langen@med.usc.edu (R.L.)
http://dx.doi.org/10.1016/j.str.2013.12.015

SUMMARY

The dynamin-related Eps15-homology domain-containing protein 2 (EHD2) is a membrane-remodeling ATPase that regulates the dynamics of caveolae. Here, we established an electron paramagnetic resonance (EPR) approach to characterize structural features of membrane-bound EHD2. We show that residues at the tip of the helical domain can insert into the membrane and may create membrane curvature by a wedging mechanism. Using EPR and X-ray crystallography, we found that the N terminus is folded into a hydrophobic pocket of the GTPase domain in solution and can be released into the membrane. Cryoelectron microscopy demonstrated that the N terminus is not essential for oligomerization of EHD2 into a membrane-anchored scaffold. Instead, we found a function of the N terminus in regulating targeting and stable association of EHD2 to caveolae. Our data uncover an unexpected, membrane-induced regulatory switch in EHD2 and demonstrate the versatility of EPR to study structure and function of dynamin superfamily proteins.

INTRODUCTION

Eps15-homology domain-containing proteins (EHDs) comprise a highly conserved dynamin-related adenosine triphosphatase (ATPase) family in eukaryotes with four members in mammals (EHD1–EHD4) and one in *Caenorhabditis elegans* (Rme-1) and *Drosophila* (Past-1) (Naslavsky and Caplan, 2011). Studies in *C. elegans* identified a function of Rme-1 in mediating the exit of cargo proteins from the endocytic recycling compartment to the plasma membrane (Grant et al., 2001), and a similar function was demonstrated for mammalian EHD1 (Lin et al., 2001; Caplan et al., 2002). Subsequently, mammalian EHDs were shown to be involved in a diverse set of membrane trafficking pathways, both emanating from the plasma membrane and internal membrane

systems (Shao et al., 2002; Naslavsky et al., 2006; Lasiecka et al., 2010). We and others demonstrated that EHD2 specifically localizes to the neck of caveolae (Stoeber et al., 2012; Morén et al., 2012; Ludwig et al., 2013), cup-shaped invaginations of the plasma membrane enriched in the protein caveolin (Parton and del Pozo, 2013). EHD2 is not required for their formation, but it stably associates with surface-connected caveolae and slows down their mobility within the plasma membrane (Stoeber et al., 2012; Morén et al., 2012).

EHDs are composed of an N-terminal extended GTPase domain (G domain), followed by a helical domain and a C-terminal Eps15-homology (EH) domain. The G domains of EHDs bind to adenine rather than to guanine nucleotides (Lee et al., 2005a; Daumke et al., 2007). X-ray structure analysis showed that the G domains of EHD2 and dynamin are structurally related (Daumke et al., 2007). Similarly to other dynamin superfamily members, EHDs can tubulate negatively charged liposomes and oligomerize in ring-like structures around them (Daumke et al., 2007; Pant et al., 2009). In the case of EHD2, this leads to a 10-fold increase of its intrinsic ATPase activity. However, the rate of stimulated ATPase activity is still two orders of magnitude lower compared with that of dynamin under similar conditions (Faelber et al., 2011), pointing to a different function or regulation of nucleotide hydrolysis in these two proteins.

G domains of EHD2 stably dimerize via a nucleotide-independent interface that is not conserved in other dynamin superfamily proteins. A second interface in the G domain promotes nucleotide-dependent assembly in dynamin and septin superfamily proteins (Schwefel et al., 2010). Dimer assembly via this nucleotide-dependent interface may mediate oligomerization of EHD2 into rings (Daumke et al., 2007). Two helical domains protrude in parallel from the G domain dimer. Based on mutagenesis, we suggested that the tips of two adjacent helical domains form a composite membrane-binding surface involving hydrophobic and positively charged residues. The C-terminal EH domains interact with linear peptide motifs containing an Asn-Pro-Phe (NPF) motif (de Beer et al., 1998). In the EHD2 dimer, EH domains bind on top of the opposing G domains and may block the nucleotide-dependent assembly interface of the G domain. Upon EHD2 assembly, the EH domains were suggested to switch to a KPFxxxNPF-containing loop in the G domain of the

CrossMark

adjacent EHD2 dimer. The KPFxxxNPF motif also mediates direct interactions with caveolae and specific caveolar targeting (Daumke et al., 2007; Morén et al., 2012).

Despite recent progress in structural studies, our previous structural analysis did not reveal the conformational changes associated with membrane binding of EHD2. These transitions are difficult to address with conventional X-ray crystallography, because liposomes cannot be included in protein crystals. Also, with nuclear magnetic resonance, structures of EHD2 oligomers, due to their large size, cannot easily be resolved. To circumvent these problems, we used a combination of site-directed spin labeling (SDSL), electron paramagnetic resonance (EPR), X-ray crystallography, cryoelectron microscopy (cryo-EM), and cell biology. We found that residues at the tip of the helical domain directly insert into membranes. Furthermore, we identified a membrane-dependent N-terminal switch that regulates cellular targeting of EHD2.

RESULTS

The Tip of the Helical Domain Is a Primary Membrane-Binding Site

Mammalian EHDs share a sequence identity of 70%–85% and display common domain architecture (Figures 1A and 1B). Based on their location in the crystal structure and on mutagenesis experiments, it has been inferred that residues at the tip of the helical domain (residues 320–340; Figure 1C) mediate membrane interaction (Daumke et al., 2007). Mutations in some of these residues reduce liposome binding and result in a cytoplasmic distribution of the protein when expressed in HeLa cells. To test whether this region recruits EHD2 to membranes via a direct membrane interaction, we established an SDSL approach in combination with EPR spectroscopy. The three internal cysteines of EHD2 were mutated to serines. This cysteine-less EHD2 still bound and tubulated liposomes (data not shown). Subsequently, six residues in the helical domains were individually replaced with a single cysteine that was then coupled to the paramagnetic spin label (1-oxyl-2,2,5,5-tetramethylpyrroline-3-methyl)methanethiosulfonate (MTSL) to generate the spin-labeled side chain R1.

EHD2 can remodel liposomes into tubules and small unilamellar vesicles (SUVs). For our studies, we used preformed SUVs composed of bovine brain lipids (Folch) as a membrane-binding template for EHD2 for two reasons. First, EHD2 binds SUVs with high affinity, even in the absence of nucleotides (Daumke et al., 2007). Second, SUVs were stable over the time course of the experiments (~30 min), resulting in a reproducible membrane-bound conformation. In contrast, EHD2-decorated tubules generated from Folch-large unilamellar vesicles (LUVs) were metastable and led to precipitation of EHD2, occluding further analysis.

First, we investigated the spectral changes of EHD2 spin labeled at position 322. Phe322 is directly located at the tip of the helical region and was previously proposed to interact with the membrane (Daumke et al., 2007). The continuous wave (CW) spectrum of F322R1 showed ordering upon addition of SUVs (Figure 1D). Addition of the nonhydrolyzable ATP analog adenosine-5′-O-(3-thio)triphosphate (ATPγS) did not induce further spectral changes (Figure 1D), in agreement with the

nucleotide-independent interaction of EHD2 with SUVs. Second, we tested whether additional sites, further away from the tip region, also exhibit mobility changes. EHD2 derivatives containing single spin labels at position 320, 321, 323, 324, or 328 also revealed ordering upon addition of SUVs (Figure 1D). In contrast, no significant mobility changes upon addition of SUVs were observed in the spectra of an EHD2 variant labeled at residue 277, a site in the G domain not expected to interact with the membrane.

To identify residues directly inserting into the membrane, accessibilities of the spin labels to paramagnetic colliders O_2 (partitions into the membrane) and nickel ethylene-di-amine-di-acetic acid (NiEDDA) (partitions into the aqueous phase) were measured. In the absence of membranes, the depth parameter Φ, defined as the logarithm of the ratio of accessibilities to O_2 and NiEDDA, showed negative values for all EHD2 variants. This result was expected because negative Φ values (e.g., high accessibility to NiEDDA) are typically observed in solution containing 10 mM NiEDDA. In the presence of liposomes, the values of positions 320, 321, 322, 324, and 328 became positive due to enhanced O_2 and reduced NiEDDA accessibilities (Figure 1E). Although all sites showed ordering with moderate reduction in mobility, none of the sites became severely immobilized by tight packing interaction. Thus, steric exclusion of NiEDDA, as can occur within protein cores (Isas et al., 2002), did not contribute to the positive Φ values. Together, these data indicated direct membrane insertion of the selected sites. Spin labels attached to position 323 and to position 277 in the G domain displayed negative values and thus do not directly insert into the membrane.

Calibrating the Φ values with spin-labeled lipids revealed that the membrane insertion depth of the nitroxide radical was between 3 and 16 Å (Figures 1E and 1F), indicating that the entire tip region inserts into the outer leaflet of the membrane. These data support the notion that this region represents an important membrane-binding site; the membrane immersion depth suggests that this region may also be able to promote membrane curvature via a wedging mechanism (Campelo et al., 2008). Due to the essential nature of this region for membrane interaction and due to its important role in membrane curvature induction, we consider this region to be a primary membrane-binding site.

The N Terminus of EHD2 Folds against the G Domain

Our previous EHD2 model starts with residue 19. Residues 1–18 were not included because there was no connecting electron density before residue 19 (Figure 1B). Interestingly, the very N-terminal residues are highly conserved (Figure 2A), indicating a conserved functionality.

To study structural and functional properties of these residues, we used our established EPR spectroscopy approach with EHD2 variants singly spin labeled at residues 2–9. CW EPR spectra of these EHD2 variants in the absence of membranes and nucleotides showed predominantly immobile components, indicating an ordered conformation (Figure 2B, open triangle). This was unexpected because the absence of the N terminus in the X-ray-derived model suggested a flexible conformation. Consistent with this notion, each site also revealed the presence of a small fraction of a highly mobile and disordered
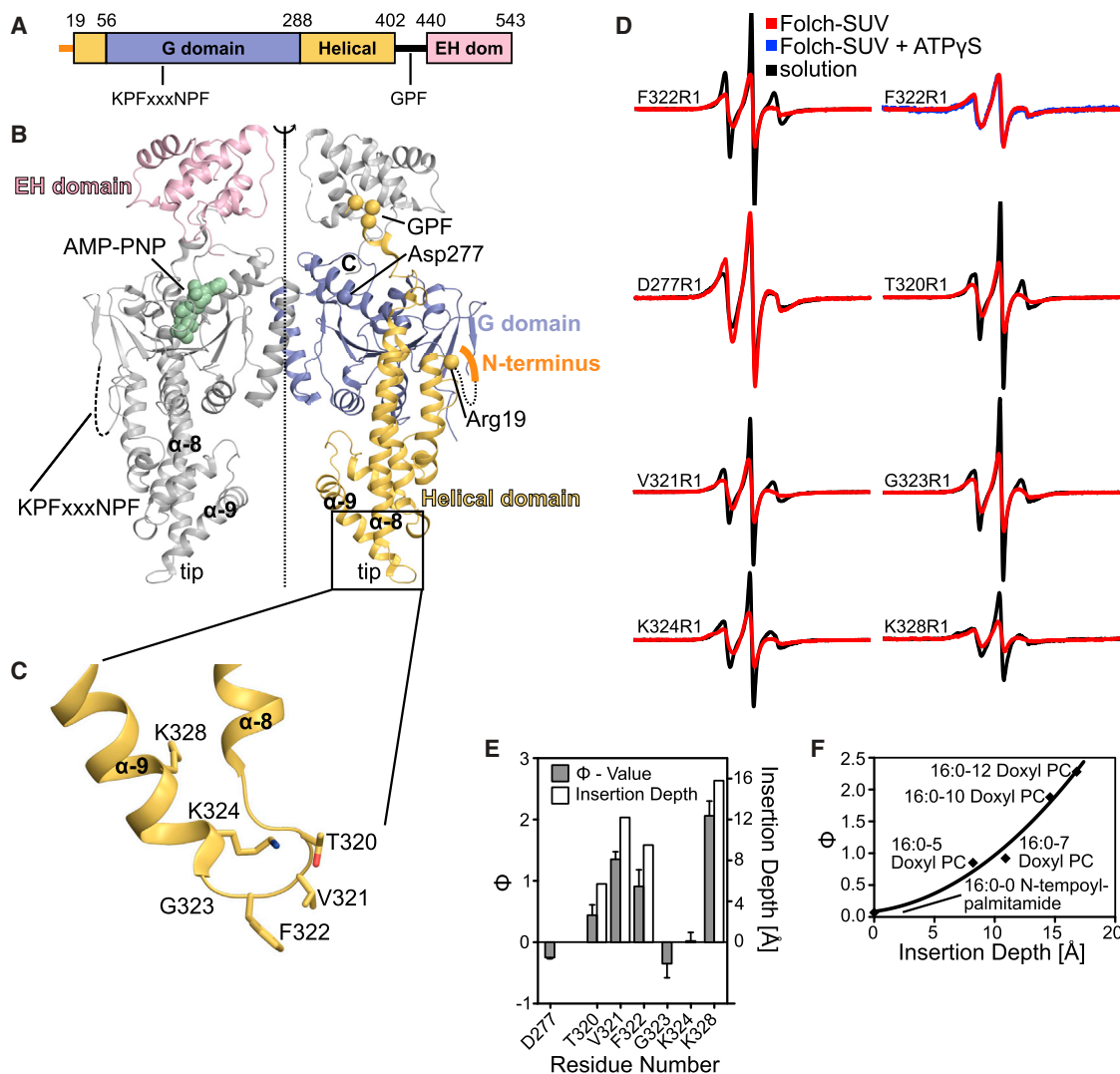
Figure 1. Identification of the Primary Membrane-Binding Site by EPR

(A) Structure-based domain architecture of EHD2. Amino acid numbers at the domain boundaries and the location of two conserved peptide motifs are indicated.

(B) Structure of the EHD2 dimer in the presence of the nonhydrolyzable ATP analog AMPPNP. The positions of the first visible amino acid in the helical domain (Arg19), a residue in the G domain (Asp277), and the KPFxxxNPF motif at the distal side of the G domain are indicated.

(C) Magnification of the boxed area in (B) showing details of the primary membrane-binding site of EHD2. Amino acids that have been modified by a spin-labeled side chain in this study are shown in stick representation.

(D) CW EPR spectra of nucleotide-free EHD2 spin labeled at residues 277, 320–324, and 328 in the absence (black) and presence (red) of Folch-SUVs. Spectra of residue 277 in the G domain of EHD2 showed no immobilization upon addition of Folch-SUVs, in contrast to the spectra of all other residues. Addition of ATPγS did not lead to further spectral changes of membrane-bound EHD2 F322R1 (blue).

(E) The logarithmic ratio Φ of the accessibilities of spin labels to the paramagnetic colliders O_2 and NiEDDA was calculated for EHD2 labeled at positions 277, 320–324, and 328 in the absence of nucleotide and presence of Folch-SUVs (solid bars referring to the left y axis). Positive Φ values indicate membrane interaction. Based on calibrations with spin-labeled lipids, the membrane insertion depth of each residue was derived (open bars refer to the right y axis; see also F). Error bars represent SEM (n = 3).

(F) Insertion depth calibration using power saturation experiments with Folch-SUVs containing 1% (w/w) of spin-labeled lipids mixed with nucleotide-free EHD2. For position 0, N-tempoylpalmitamide, and for positions 5, 7, 10, and 12, the respective 1-palmitoyl-2-stearoyl-(n-doxyl)-sn-glycero-3-phosphocholines (Doxyl PC) were used. Each position corresponds to an insertion depth taken from Altenbach et al. (1994) and Oh et al. (2010). The Φ values could be fitted with a polynomial regression.

conformation (Figure 2B, closed triangle). Substitution of the hydrophobic amino acids Phe2, Trp4, and Leu5 with R1 resulted in larger percentages of mobile components (Figure 2B) and smaller percentages of immobile components (Figure 2C) compared with the other N-terminal sites. Thus, the hydrophobic

residues might contribute to the stabilization of the ordered conformation of the N terminus, perhaps by interaction with a hydrophobic binding pocket.

To locate the position of the N terminus, double electron-electron resonance (DEER) distance measurements were performed
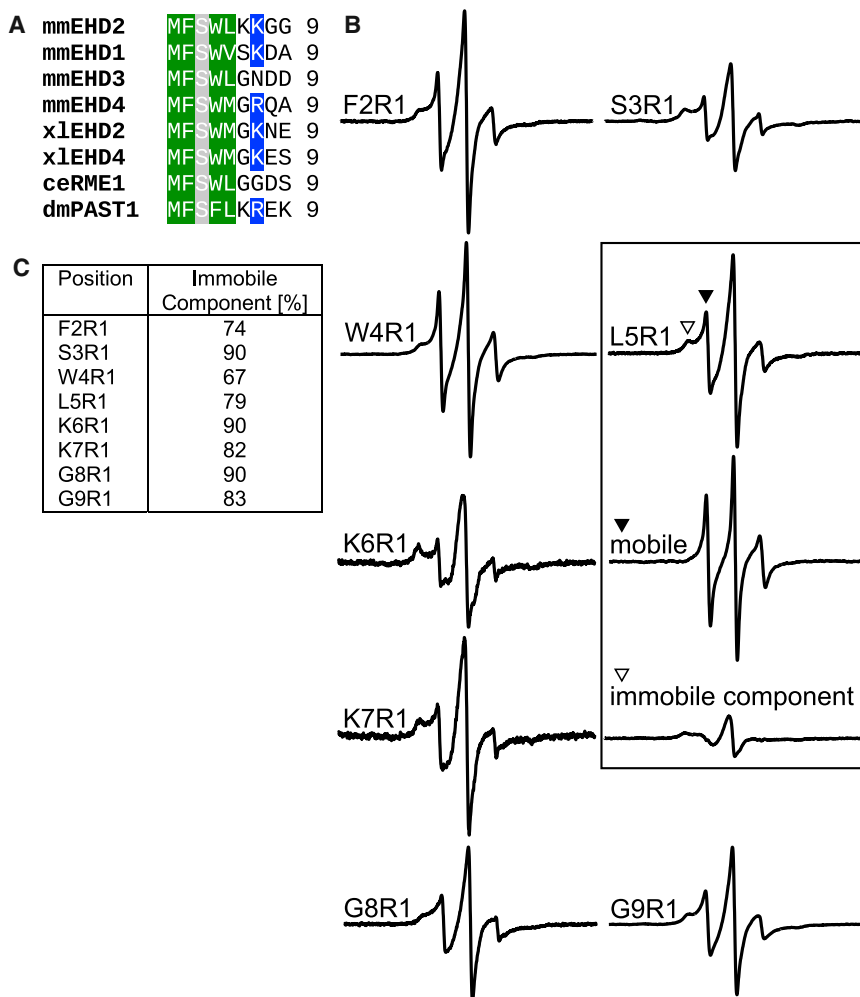
A

mmEHD2	MFSWLKKGG	9
mmEHD1	MFSWVSKDA	9
mmEHD3	MFSWLGNDD	9
mmEHD4	MFSWMGRQA	9
xlEHD2	MFSWMGKNE	9
xlEHD4	MFSWMGKES	9
ceRME1	MFSWLGGDS	9
dmPAST1	MFSFLKREK	9

B

F2R1   S3R1

W4R1   L5R1 ▽ ▼

K6R1   ▼ mobile

K7R1   ▽ immobile component

G8R1   G9R1

C

Position	Immobile Component [%]
F2R1	74
S3R1	90
W4R1	67
L5R1	79
K6R1	90
K7R1	82
G8R1	90
G9R1	83

Figure 2. The N Terminus Is in an Ordered Conformation in Solution

(A) Sequence alignment of amino-terminal residues in the EHD family. Conserved hydrophobic residues are marked in green, positively charged residues in blue, and serines in gray.

(B) CW EPR measurements of nucleotide-free EHD2 spin labeled at positions 2–9. As exemplified for L5R1 (boxed), all spectra can be separated into a small fraction of mobile component (filled triangle) and a predominant immobile component (open triangle).

(C) Table listing the fraction of immobile spectral components of residues 2–9, based on CW EPR measurements from (B).

Using the refined phases, the improved resolution of this data set, and the additional SeMet signal, we assigned the N-terminal seven residues of EHD2 into this electron density (Figures 3D and 3E). As predicted by the DEER data, the N terminus binds back to the G domain. Further in agreement with the EPR spectra, we found that the N terminus packs into a mostly hydrophobic binding pocket (Figure 3E). In addition to the N-terminal residues, seven residues belonging to the spatially adjacent KPFxxxNPF loop were built in the refined electron density. Interestingly, the N terminus is in proximity to the NPF sequence of this loop and makes physical contact with amino acids that are flanking the loop region (Figure 3F). By bridging the KPFxxxNPF loop region to the G domain, the N terminus may regulate the ability of the KPFxxxNPF region to interact with other binding partners (see below).

The N Terminus Can Insert into Membranes, but Is Not Essential for Membrane Binding and Oligomerization

A recurring theme in membrane curvature-inducing proteins is that N-terminal regions can undergo conformational reorganization and make contact with the membrane, for example, in N-BAR proteins (Gallop et al., 2006), epsin (Boucrot et al., 2012), and Arf GTPases (Lee et al., 2005b). To test whether such a mechanism might also apply to EHD2, we used EPR spectroscopy of spin-labeled EHD2 variants in the presence of membranes. Similarly to residues in the primary membrane-binding site, N-terminally labeled EHD2 variants underwent spectral changes upon membrane binding. The N-terminal labeling sites (positions 2–9) lost their highly mobile and highly immobile spectral components upon SUV binding, and the EPR spectra were instead dominated by spectral components with intermediate mobility (Figure 4A). This suggests an ordered, but not tightly packed conformation of this N-terminal sequence stretch in the presence of membranes. The lack of packing interactions also requires a release from the binding pocket in the G
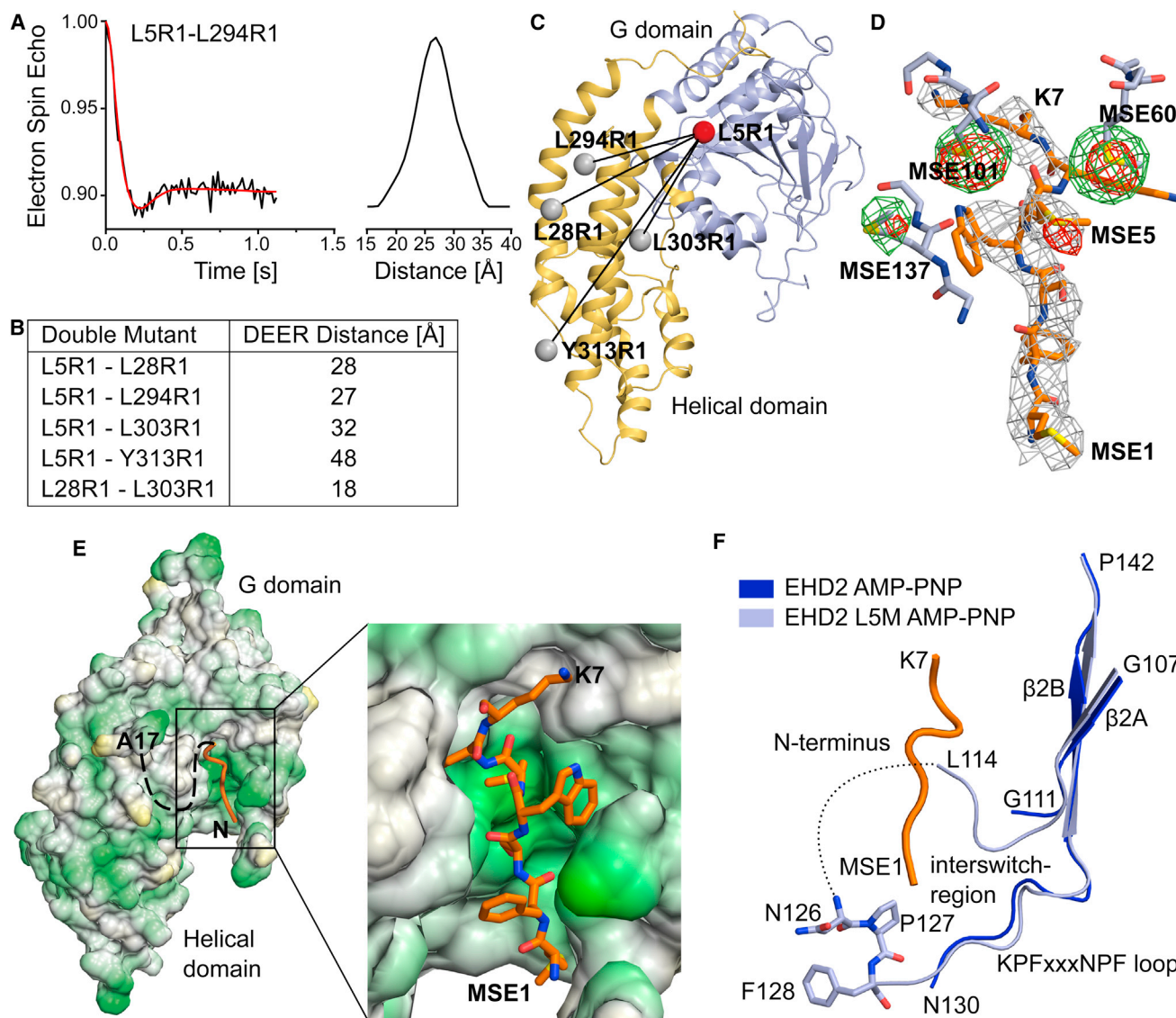
using EHD2 variants spin labeled at position 5 in the N terminus and an additional residue in the helical domain (Figures 3A and 3B; Figure S1 available online). Distances between residues 5 and 28, 5 and 294, 5 and 303, and 5 and 313 ranged from 27 to 48 Å (Figure 3B). As a control, the distance between residues 28 and 303 within the helical domain was determined to be 18 Å, consistent with the predicted distance derived from the crystal structure. The position of residue 5 was derived by a trilateration method (Figure 3C). This approach indicated that Leu5 is located in proximity to the G domain.

To accurately determine this position, Leu5 was mutated to methionine, and a selenomethionine (SeMet)-derivatized EHD2 variant was crystallized in the presence of the nonhydrolyzable ATP analog adenylyl-imidodiphosphate (AMPPNP). SeMet5 gave rise to an additional signal in an anomalous difference Fourier map (Figure 3D; Table 1). Interestingly, the position of this signal was within a previously unexplained electron density patch in a conserved hydrophobic groove at the distal side of the G domain. Previously, the electron density could not be assigned to the EHD2 sequence, due to the limited resolution of the data set, missing connectivity, only partial occupancy (as suggested by EPR), and the presence of two disordered loops in this region.

Figure 3. The N Terminus Binds in a Hydrophobic Pocket of the G Domain

(A) Representative example of a distance measurement between Leu5R1 and Leu294R1, using pulsed EPR measurements in the absence of nucleotides. See Figure S1 for other distance measurements.

(B) Table listing distances between different pairs of spin labels, determined by DEER.

(C) Based on the predicted position of the spin labels (gray balls) and four EPR distance pairs, the position of Leu5 (red ball) was determined to be close to the G domain.

(D) The N terminus (residues 1–7) was modeled in the $2F_o$-F_c density, contoured at 1σ, derived from the AMPPNP-bound EHD2 Leu5SeMet data set. The anomalous signals (contoured at 4σ) derived from AMPPNP-bound SeMet-labeled EHD2 Q410A (green) and EHD2 L5M Q410A (red) are superposed. Nearby residues from the G domain are shown as stick representations, without $2F_o$-F_c density. An additional anomalous signal for SeMet5 is apparent.

(E) Hydrophobic surface representation of the G and helical domains of EHD2. Green represents hydrophobic residues and yellow hydrophilic residues. The N-terminal sequence stretch (orange) binds into a hydrophobic pocket of the G domain. The boxed area is shown in more detail on the right.

(F) Superposition showing the KPFxxxNPF loop from EHD2 Q410A (blue, PDB code: 2QPT) and EHD2 L5M Q410A (light blue). The N terminus is shown in orange. Seven previously unresolved residues in the KPFxxxNPF loop region were modeled in the refined electron density.

domain. Thus, the membrane-bound state of the N terminus represents a third state that is ordered and distinctively different from the two states observed in solution. Spin labels attached at positions 2, 5, 6, 7, 8, and 9 showed positive Φ values upon liposome addition, indicating membrane insertion (Figure 4B). However, spin labels attached to positions 3 and 4 in the N-terminal membrane-binding site had negative values, indicating no membrane penetration. Based on our previous calibration (Figure 1F), we conclude that the N terminus undergoes shallow insertion into the outer membrane monolayer.

Although the N terminus could bind to membranes, it was not essential for the interaction with liposomes. In liposome

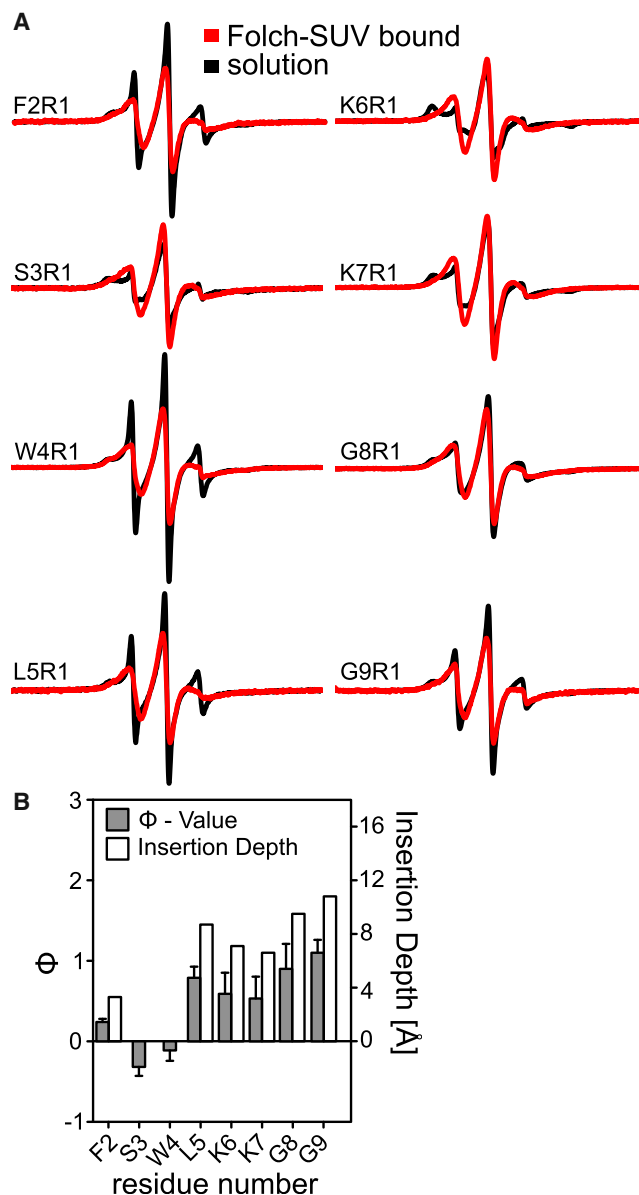**Table 1. Data Collection and Refinement Statistics**

	mmEHD2 L5M Q410A SeMet[a]
Data Collection	
Space group	C2
Cell dimensions	
a, b, c (Å)	99.9, 134.7, 56.1
α, β, γ (°)	90.0, 106.1, 90.0
Beamline	BESSY II MX-14.1
Wavelength (Å)	0.97969
Total reflections	42,946 (4,095)
Unique reflections	26,426 (2,552)
Resolution (Å)	40–3.0 (3.1–3.0)
R_{obs} (%)	4.7 (33.9)
R_{meas} (%)	6.7 (47.8)
$I/\sigma I$	10.5 (1.8)
Completeness (%)	95.9 (98.0)
Redundancy	1.6 (1.6)
Wilson B-factor (Å^2)	76
Refinement	
Resolution (Å)	40–3.0 (3.078–3.0)
No. reflections	13,424 (989)
R_{work}/R_{free} (%)	23.0/27.9 (33.8/37.8)
No. of atoms	
Protein	3,958
Nucleotide	31
Metal ions	2
Water	4
Averaged B-factor protein (Å^2)	84
Root mean square deviations	
Bond lengths (Å)	0.005
Bond angles (°)	1.027

[a]Numbers in parentheses represent values from the highest resolution shell.

Figure 4. The N Terminus Can Insert into Membranes

(A) CW EPR spectra of nucleotide-free EHD2 spin labeled at residues 2–9 in the absence (black) and presence (red) of Folch-SUVs.

(B) Similarly as in Figure 1E, Φ and the insertion depth for EHD2 spin labeled at positions 2–9 was determined. At positions 6 and 7, the spin label might insert deeper into the membrane compared with the corresponding lysines that may snorkel in the membrane. Error bars represent SEM (n = 3).

cosedimentation assays, EHD2 bound with similar efficiency to LUVs as an EHD2 variant without the N-terminal 18 residues (EHD2[19–543]) (Figure 5A). We therefore consider the N-terminal region as a secondary membrane-binding site that may modulate membrane interaction.

To probe the tubulation potential of EHD2, cryo-EM was used. In the absence of ATP, EHD2 efficiently bound to Folch-LUVs. However, this resulted only in weak liposome tubulation (Figure 5B). Only in the presence of ATP did EHD2 significantly tubulate liposomes and form a highly regular oligomeric EHD2 scaffold (Figures 5C and 5D). Quantification of the average tubule diameter indicated a narrow size distribution of EHD2-coated tubules (51 ± 3.8 nm) (Figure 5E).

In the presence of ATP, EHD2[19–543] also efficiently deformed liposomes into tubules of similar diameter that were decorated by an ordered protein coat (Figure 5D). This indicates that the N terminus of EHD2 is not required for membrane tubulation and oligomerization. However, the N-terminally truncated variant showed a broader size distribution of the tubule diameter (Figure 5E). This may point to a role of the N terminus in the formation

of defined oligomeric assemblies on membranes. Regardless of these subtle structural differences, a specific highly oligomeric protein coat could be observed in both cases, supporting the notion that scaffolding is an important aspect of EHD2's ability to induce membrane curvature.

The N-Terminal Residues Control the Localization and Stability of EHD2 Oligomers in Cells

Having established that the N terminus of EHD2 undergoes a major conformational change upon membrane interaction that
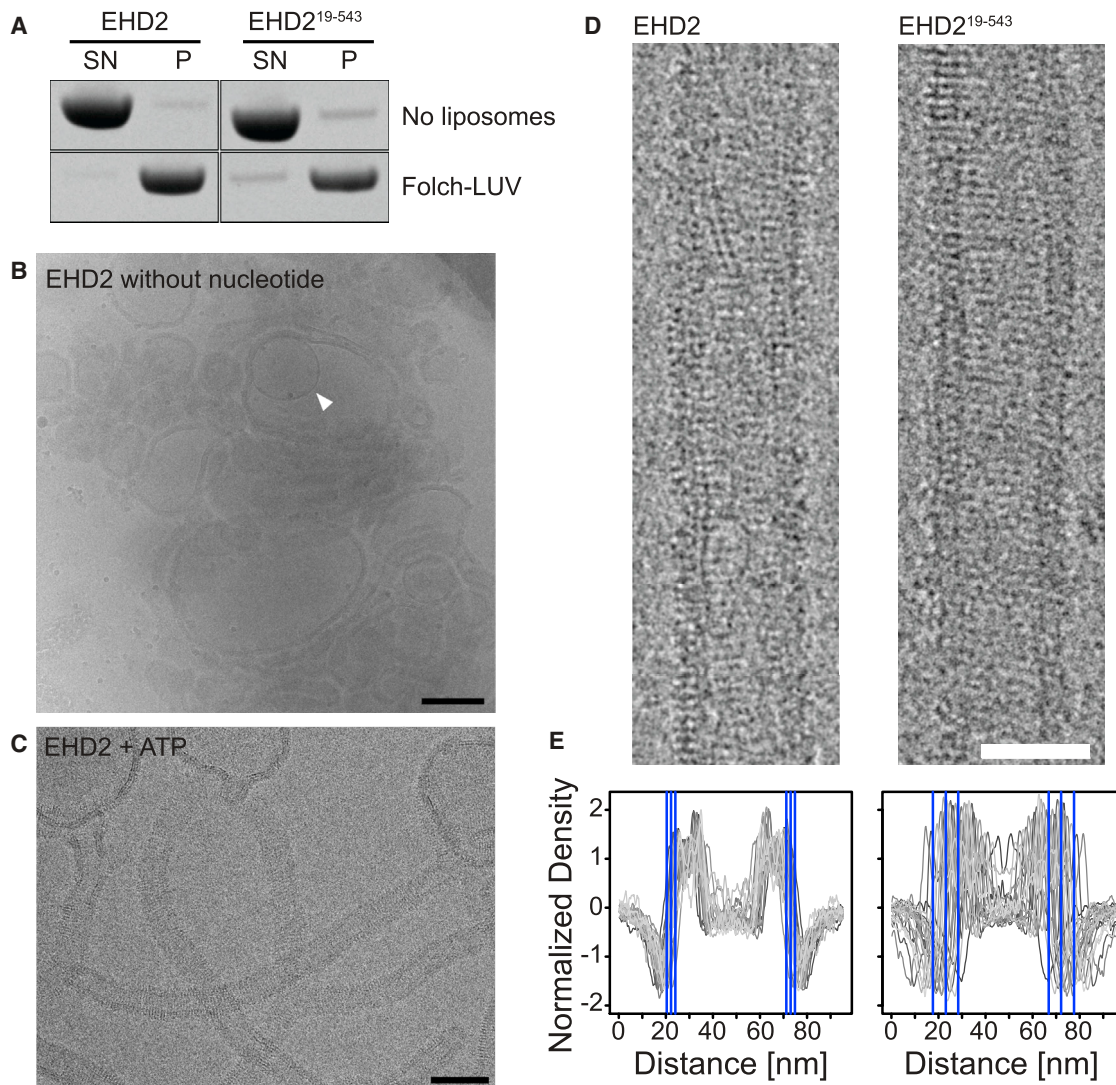
Figure 5. The N Terminus Does Not Affect Membrane Binding and Oligomerization

(A) Cosedimentation assays of EHD2 and EHD2$^{19–543}$ in the absence (top) and presence (bottom) of 800-nm-filtered Folch-LUVs, without addition of nucleotides. P, pellet fraction; SN, supernatant.

(B and C) Cryo-EM of EHD2 in the presence of 800 nm Folch-LUVs and absence of nucleotide (B) and in the presence of ATP (C). Inner vesicles of occasional multilamellar vesicles (B, white arrow) were shielded from the EHD2-containing buffer and showed typical bilayer structures, indicating that the surrounding liposomes were densely coated by EHD2. Similarly to cryo-EM micrographs of dynamin (Danino et al., 2004), we did not observe an accumulation of small vesicles, suggesting that EHD2 is not fragmenting liposomes under these conditions. Scale bars, 200 nm (B) and 100 nm (C).

(D) Cryo-EM images of membrane tubules decorated with EHD2 and EHD2$^{19–543}$ were prepared by incubating EHD2 with Folch-LUVs in the presence of ATP. Regular patterns, most likely corresponding to ordered assemblies of the protein on the lipid tubule surface, were observed for both constructs. Scale bar, 50 nm.

(E) 1D density profiles of membrane tubules decorated with EHD2 and EHD2$^{19–543}$. In EHD2, the average outer diameter of protein-coated tubules was similar (d = 51 ± 4 nm, n = 2,156), as shown by the small SD. Deletion of the N terminus had little effect on the average outer diameter of the tubules (d = 49 ± 11 nm, n = 1,081), but significantly increased the spread. The lines in the 1D profile indicate the average outer limit of the tubes ± 1 SD.

is not essential for membrane binding and tubulation in vitro, we next asked about the functional significance of the N terminus in living cells. We previously showed that EHD2 fused to an N-terminal EGFP-tag extensively colocalized with caveolae when overexpressed in 3T3-L1 fibroblasts (Morén et al., 2012). Due to the spatial proximity and its size, we suspected that an N-terminal tag might mask the functionality of the N-terminal residues. To overcome this problem, we overexpressed a C-terminally Cherry-tagged EHD2 construct (EHD2-Cherry) in

3T3-L1 cells. In agreement with previous data (Stoeber et al., 2012), this construct showed a more diffuse and cytoplasmic distribution than N-terminally tagged EHD2 and only partly associated with GFP-tagged caveolin (Figure 6A). These results indicate that N- or C-terminal tags can influence membrane recruitment and/or oligomerization of EHD2. In contrast to EHD2-Cherry, an N-terminally truncated EHD2 variant (EHD2$^{19–543}$-Cherry) was found in big clusters and tubes positive for caveolin, with almost no cytoplasmic pool (Figure 6B). This
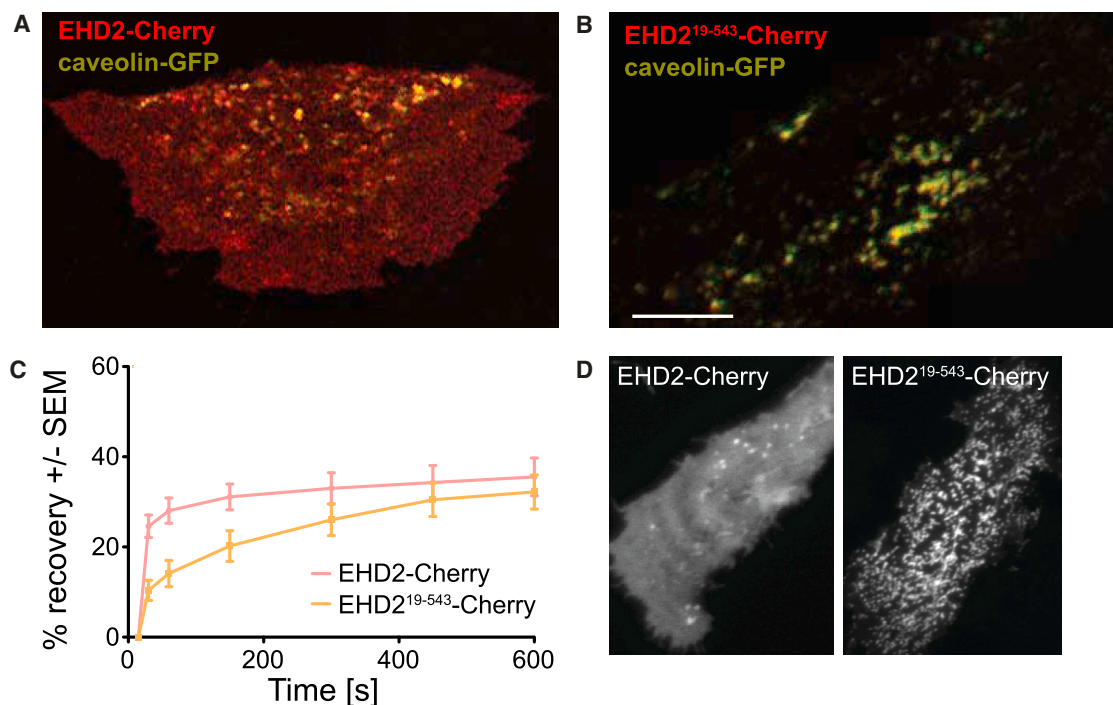
Figure 6. The N Terminus of EHD2 Directs Caveolar Targeting
(A and B) Fluorescent confocal micrographs of 3T3-L1 cells expressing EHD2-Cherry (A) or EHD2$^{19–543}$-Cherry (B) together with caveolin-GFP. Scale bar, 10 μm.
(C) Quantification of FRAP microscopy of 3T3-L1 fibroblasts from (A) and (B). For this, distinct caveolae enriched in EHD2-Cherry and caveolin-GFP were bleached, and the time-dependent recovery of EHD2 fluorescence in this area was traced over 10 min. The graphs show recovery of fluorescence, as quantified from three independently bleached regions in three to five cells. Error bars represent SEM.
(D) Fluorescent confocal micrographs of HeLa cells expressing EHD2-Cherry or EHD2$^{19–543}$-Cherry. Scale bar, 10 μm.

suggested that EHD2$^{19–543}$-Cherry associates more stably with caveolin-positive structures than EHD2-Cherry. This was subsequently confirmed in fluorescence recovery after photobleaching (FRAP) experiments (Figure 6C).

In HeLa cells, EGFP-EHD2 has been shown to tubulate membranes, probably due to the low abundance of caveolin in these cells and the tendency of EGFP-EHD2 to oligomerize at membrane surfaces (Morén et al., 2012). Here, we used HeLa cells to study the role of the N terminus in membrane recruitment. Similarly as in 3T3-L1 fibroblasts, EHD2-Cherry localized to the cytoplasm and to discrete punctae representing caveolae (Figure 6D, left). In contrast, EHD2$^{19–543}$-Cherry was hardly found in the cytosol, but it formed an interconnected tubular membrane network at the cell surface, indicative of more stable membrane association (Figure 6D, right). These data suggest that the N terminus constitutes a switch region that controls membrane recruitment of EHD2.

DISCUSSION

The large size, multidomain nature, and oligomerization of dynamin superfamily proteins make their structural and functional characterization challenging. In particular, structures of membrane-bound oligomerized forms of these proteins are difficult to characterize. To overcome these hurdles and elucidate structural features of membrane-bound EHD2, we used a combination of methods, including EPR, X-ray crystallography, cryo-

EM, and cellular imaging. This study details the application of EPR to a member of the dynamin superfamily, whose proteins are significantly larger than most other proteins typically studied by EPR. Our data suggest that analogous approaches can be applied for structural studies of other membrane-bound protein systems of similar complexity.

Our structural analysis of soluble EHD2 revealed a previously unknown three-state nature of the N-terminal switch region. When EHD2 is in solution, the predominant conformation of this region is a highly ordered state that is stabilized by specific interactions with the G domain. In addition, the N terminus can also exist in a highly dynamic, unfolded state in solution. Finally, a third conformational state with intermediate conformational flexibility was observed in the presence of membranes. This conformational flexibility of the N terminus, as identified by a combination of EPR and X-ray crystallography, is likely a prerequisite for its function as a cellular regulatory switch. Intriguingly, point mutations in the N-terminal region of *C. elegans* Rme-1 prevent the exit of proteins from the endocytic recycling compartment, showing the functional importance of this region (Grant et al., 2001).

To characterize the membrane-bound state of EHD2, we also performed cryo-EM studies of EHD2-decorated membrane tubules. This approach resolved a highly defined and periodic coat of EHD2 proteins wrapped around the tubular membrane. These data support the previously proposed notion (Daumke et al., 2007) that EHD2 oligomers act as scaffolds that induce

membrane curvature, similarly as reported for BAR proteins (Frost et al., 2008; Mim et al., 2012; Mizuno et al., 2010). It was previously found that residues at the tip of the helical domain are essential for membrane interaction in vitro and in vivo (Daumke et al., 2007). Interestingly, our EPR data demonstrate that these residues do not simply anchor the protein to the membrane but that several residues directly penetrate into the membrane. Based upon theoretical considerations (Campelo et al., 2008), this insertion may help to further promote membrane curvature through a wedging mechanism. The concerted use of scaffolding and wedging is not without precedent because amphipathic helices and scaffolding domains are thought to act together in the N-BAR proteins endophilin and amphiphysin (Gallop et al., 2006). Due to this importance of the tip of the helical domain in membrane binding and curvature induction, we consider this region to be a primary membrane-binding site.

The shallow insertion of the N terminus seen by EPR depth measurements suggests that this region could also act as a wedge or a membrane curvature sensor. However, in contrast to the membrane insertion of the primary membrane-binding site, the N-terminal region is not essential for tubulation and membrane remodeling of liposomes. This makes it unlikely that the N terminus plays an important wedging function. Instead, our cellular data indicate that the N terminus plays a regulatory role in caveolar targeting. In the absence of the N terminus, EHD2 forms an interconnected membranous network at the cell surface that might result from altered properties of its recruitment, oligomerization, or membrane-remodeling activity. The physiological significance of this network, if any, is unclear.

What could be the mechanism for such functions? In the absence of membranes, the predominant, ordered form of the N terminus is at a significant distance from the membrane-interacting tip of the helical domain. Nonetheless, our data indicate that the N terminus can move away from its binding pocket in the G domain toward the membrane. This movement will disrupt the contact between the N terminus and the KPFxxxNPF loop and its flanking region that is formed in solution. It has previously been suggested that oligomerization is promoted by an interaction of the EH domains from one dimer with the KPFxxxNPF loops of neighboring dimers (Daumke et al., 2007; Morén et al., 2012). Accordingly, deletions of the EH domain or mutations in the KPFxxxNPF motif reduce oligomerization of EHD2. We propose that a membrane-mediated movement of the N terminus induces a conformation of the KPFxxxNPF loop that makes it competent to bind the neighboring EH domain. In this case, the N terminus would act as a switch that senses membrane proximity, membrane curvature, or both, and its movement would help to promote oligomerization. In addition, the N terminus might directly interact with partner molecules at caveolae. Further experiments are required to test this hypothesis.

The N terminus of EHD2 has similarities but also some differences compared with small G proteins of the Arf family (Lee et al., 2005b; Pucadyil and Schmid, 2009; Lundmark et al., 2008; Krauss et al., 2008). It binds into a hydrophobic groove of the G domain in both cases. However, in small G proteins, guanosine triphosphate binding triggers the release of the N-terminal amphipathic helix into the membrane. This helix promotes

membrane curvature, likely via a wedging mechanism. In contrast to small G proteins, our current analysis of EHD2 did not provide evidence for an interplay between nucleotide binding and release of the N terminus, and it did not indicate a function as membrane wedge. Moreover, unlike in the N-terminal regions of membrane-bound epsin (Lai et al., 2012) and endophilin (Jao et al., 2010), the Φ values of labeled N-terminal sites of EHD2 did not reveal a clear periodicity that would correspond to a stable α-helical structure. This finding may not be too surprising because the N terminus of EHD2 contains two glycine residues at positions 8 and 9 that would likely destabilize an α helix. Also PACSINs interact with the membrane via a wedge loop (Wang et al., 2009), a region also lacking distinctive secondary structure.

Similarly to EHD2, most members of the dynamin superfamily interact with membranes via a primary membrane-binding motif located at the tip of their helical domains. This was shown, for example, for the pleckstrin homology domain of dynamin, and for other membrane-binding motifs in dynamin-like myxovirus resistance (Mx) protein A (von der Malsburg et al., 2011), bacterial dynamin-like protein (Low et al., 2009), and the membrane fusion GTPase atlastin (Liu et al., 2012). However, additional N-terminal membrane-binding sites might also be present in other dynamin superfamily members. For example, a long isoform of dynamin-like optic atrophy 1 has a predicted transmembrane helix at the N terminus that might act as a secondary membrane-binding site. Also Mx proteins, guanylate binding proteins, and BDLP, but not dynamin, have long N-terminal extensions of unknown function that may contribute to membrane interaction (Praefcke and McMahon, 2004). Thus, we envisage that the mechanism of N-terminal membrane-inserting sequences is a common theme in dynamin superfamily proteins.

EXPERIMENTAL PROCEDURES

Protein Expression and Purification

Full-length mouse EHD2 and all mutant constructs, including the SeMet-substituted protein, were expressed as N-terminal His$_6$-tag fusions in *Escherichia coli* Rosetta 2 (DE3) (Novagen) and were purified as described previously (Daumke et al., 2007). EGFP- and Cherry-tagged variants of EHD2 were cloned into pEGFP-C3 and pmCherry-N1 (Clontech Laboratories), respectively. The monomeric red fluorescent protein- and EGFP-tagged caveolin1 plasmids were purchased from Addgene (14434 and 27704).

Crystallization and Structure Determination

Crystallization trials by the sitting-drop vapor-diffusion method were performed at 4°C using a Hydra-II pipetting robot (Thermo Scientific). We mixed 300 nl of SeMet-substituted mmEHD2 L5M Q410A at a concentration of 20 g/l in the presence of 2 mM AMPPNP (Jena Bioscience) and 4 mM MgCl$_2$ with an equal volume of reservoir solution containing 100 mM MES buffer (pH 6.5), 4% polyethylene glycol 3350, 5% 2-methyl-2,4-pentanediol (MPD), and 20 mM MgCl$_2$. Tetragonal crystals grew within 4 days. Crystals were cryo-protected in two steps by transferring them into buffer containing 50 mM MES buffer (pH 6.5), 75 mM NaCl, 4 mM MgCl$_2$, 5 mM AMPPNP, and 14% or 27% MPD and flash-freezing in liquid nitrogen. Diffraction data from a single crystal were recorded at BL14.1 at Berliner Elektronenspeicher-ring-Gesellschaft für Synchrotronstrahlung (BESSY) II and processed using the XDS program suite (Kabsch, 2010). Crystals were isomorphous to those previously obtained for the mmEHD2 Q410A mutant (Protein Data Bank [PDB] code: 2QPT) (Daumke et al., 2007). Experimental phases were calculated from single-wavelength anomalous diffraction using Sharp (Bricogne

et al., 2003). Model building was done in COOT (Emsley et al., 2010). Translation/libration/screw motion anisotropy and restrained refinement was carried out with Refmac5 (Murshudov et al., 2011). All residues were in the allowed regions of the Ramachandran plot, as assessed by COOT. Figures were prepared with PyMol (Schrödinger), and sequences were aligned using Clustal W (Larkin et al., 2007).

Liposome Preparation
Folch fraction I bovine brain lipids (Sigma-Aldrich) were dissolved in chloroform, dried under gentle argon stream, and desiccated overnight. EPR experiments were performed with SUVs. SUVs at a final concentration of 20 g/l were obtained by hydrating 5 mg of Folch lipids in 250 μl of 20 mM 4-(2-hydroxyethyl)-1-piperazineethanesulfonic acid (HEPES) (pH 7.5) and 300 mM NaCl and tip sonicating until the solution turned clear. For the liposome cosedimentation assay, LUVs at a final concentration of 4 g/l were obtained by hydrating 1 mg of Folch lipids in 250 μl of 10 mM HEPES (pH 7.5), 2.4 mM KCl, and 1 mM EDTA and filtering 11 times through 800-nm-pore-size polycarbonate membranes in a mini-extruder (Avanti Polar Lipids). For cryo-EM, Folch-LUVs were prepared by hydration to a final concentration of 4 g/l in 10 mM HEPES (pH 7.5), 150 mM NaCl, 1 mM MgCl$_2$, and 2.5 mM dithiothreitol (DTT). The hydrated lipids were vigorously vortexed and then subjected to five freeze-thaw cycles and filtered 21 times through 800-nm-pore-size polycarbonate membranes.

Spin Labeling
DTT was removed from single or double cysteine mutants using PD-10 columns (GE Healthcare) equilibrated with 20 mM HEPES (pH 7.5) and 300 mM NaCl. Five-time molar excess of spin label MTSL (Toronto Research Chemicals) was added and reacted with the cysteines at 4°C overnight, resulting in residue R1. Excess spin label was removed using PD-10 columns, and spin-labeled proteins were flash-frozen and stored at −80°C.

CW EPR Experiments
CW EPR spectra of EHD2 in solution at a concentration of ∼2 g/l were recorded on an X-band CW EPR spectrometer (Bruker) fitted with an ER4119HS resonator at 12.7-mW-incident microwave power at room temperature (RT). Liposome-bound samples were produced by incubating 50 μg of spin-labeled protein with 1.5 mg of Folch-SUVs (1:30 [w/w] protein-to-lipid ratio) at RT for 20 min. SUV-bound EHD2 was separated from unbound EHD2 by centrifugation (152,800 × g, 20 min, 22°C). The pellet was resuspended in 20 mM HEPES (pH 7.5) and 300 mM NaCl, and spectra were recorded as described above. Accessibilities to O$_2$ (from air, Π_{Ox}) and 10 mM NiEDDA (Π_{NiEDDA}) were obtained from power saturation experiments using an ER4123D dielectric resonator (Bruker). The depth parameter Φ was calculated from $\Phi = \ln[\Pi_{Ox}/\Pi_{NiEDDA}]$ (Altenbach et al., 1994). The membrane insertion depth was obtained by calibrating Φ using N-tempoylpalmitamide (gift from Kyoung Joon Oh) for position 0 and 1-palmitoyl-2-stearoyl-(n-doxyl)-sn-glycero-3-phosphocholine (Avanti) with spin labels attached at carbons 5, 7, 10, and 12 (Altenbach et al., 1994; Oh et al., 2010).

Pulse EPR and Distance Measurements
To obtain the distance between spin labels, four pulse DEER (Pannier et al., 2000) experiments were performed at 78 K on an Elexsys E580 X-band pulse EPR spectrometer (Bruker) fitted with a 3-mm-split ring (MS-3) resonator, a continuous-flow cryostat (CF935, Oxford Instruments), and a temperature controller (ITC503S, Oxford Instruments). Samples of EHD2 Leu5R1 Leu28R1, EHD2 Leu5R1 L294R1, EHD2 Leu5R1 Leu303R1, EHD2 Leu5R1 Tyr313R1, and EHD2 Leu28R1 Leu303R1 were mixed with an equal amount of cysteine-less EHD2 to reduce background from intermolecular distances, cryoprotected in 15%–20% sucrose, flash-frozen, and measured. The data were fitted using Tikhonov regularization (Chiang et al., 2005) as implemented in DEERAnalysis 2011 (Jeschke and Polyhach, 2007).

Determining the Position of Residue 5 by EPR
Residue R1 can adopt several conformations. We predicted sterically and stereochemically allowed positions of R1 using PRONOX (Hatmal et al., 2012). The position of nitroxide radical was calculated by averaging the probability-weighted predicted positions. The unknown position of Leu5R1 was deter-

mined as the intersection of four spheres with the predicted spin label position as midpoints and the DEER distances as radii with a Python script (Script S1).

Liposome Cosedimentation Assay
We incubated 10 μM EHD2 with 1 g/l Folch-LUVs in 20 mM HEPES (pH 7.5), 300 mM NaCl, and 0.5 mM MgCl$_2$ for 10 min at RT and centrifuged (200,000 × g, 10 min, 25°C, TLA100). Pellet and supernatant were analyzed by SDS-PAGE.

Cryo-EM and Diameter Measurements
We equilibrated 160 μM mmEHD2 or mmEHD2$^{19-543}$ in 10 mM HEPES (pH 7.5), 150 mM NaCl, 1 mM MgCl$_2$, and 2.5 mM DTT either supplemented with 2.25 mM ATP (Carl Roth) or without added nucleotide for 5 min at RT, and then we mixed 1:1 (v/v) with Folch-LUVs. The resulting mixture (1.125 mM ATP, 80 μM mmEHD2, and 2 g/l Folch liposomes) was incubated for 15 min at RT before vitrification by flash freezing in liquid ethane on carbon-coated grids (Quantifoil) using a Vitrobot device (FEI). Images were automatically collected under minimal dose conditions using the Leginon system (Suloway et al., 2005) on a 120 kV Tecnai Spirit transmission electron microscope (FEI) equipped with an Eagle 2k charge-coupled device camera (FEI) or on a Tecnai G2 Polara microscope (FEI) operating at 300 kV equipped with a TemCam-F416 4k CMOS camera (TVIPS). Nominal magnifications were 42,000× and 39,000×, respectively. To determine diameters, individual straight and nonoverlapping tubules were manually selected using e2helixboxer from EMAN2 (Tang et al., 2007). To account for the low persistence length, each tubule was segmented into overlapping square windows with a length of 95 Å. Each segment was then individually aligned parallel to the y axis based on its layer lines and centered on the x axis based on its one-dimensional (1D) density profile. Both steps were performed iteratively using the vector from tubule selection as the starting point until convergence was reached. Final rotations and shifts were applied and manually verified before a combined 1D density profile along the x axis was calculated for each selected tubule from its segments. All alignment steps were performed in SPARX using custom scripts (Hohn et al., 2007).

Cell Biology and Microscopy
The 3T3-L1 and HeLa cells were grown in DMEM (Gibco) supplemented with 10% fetal calf serum and transfected using Lipofectamine 2000 (Life Technologies) for transient protein expression. For immunofluorescence analysis, 3T3-L1 cells were fixed in 3% paraformaldehyde in PBS for 20 min at RT and then washed and blocked in 5% goat serum with 0.05% saponin in PBS before staining with the appropriate antibodies in 1% goat serum and 0.05% saponin in PBS using standard protocols. For live-cell confocal microscopy, cells were grown and transfected according to standard protocols on uncoated MatTek dishes and then placed in a temperature-controlled chamber at 37°C with 95% air/5% CO$_2$ and 100% humidity (Okolab). Live-cell imaging data were acquired using a fully motorized inverted microscope (A1 R laser scanning confocal microscope, Nikon) using a 60× lens (Plan Apochromat VC oil, Nikon) under control of the NIS-Elements microscope imaging software (Nikon). For FRAP experiments, the region of interest was photobleached for 10 s using a 488 nm laser. Single images were taken every 10 s before and after photobleaching, and recovery intensity was measured for a total of 10 min. Time points were analyzed using NIS-Elements microscope imaging software and Prism (GraphPad).

REFERENCES

Altenbach, C., Greenhalgh, D.A., Khorana, H.G., and Hubbell, W.L. (1994). A collision gradient method to determine the immersion depth of nitroxides in lipid bilayers: application to spin-labeled mutants of bacteriorhodopsin. Proc. Natl. Acad. Sci. USA 91, 1667–1671.

Boucrot, E., Pick, A., Çamdere, G., Liska, N., Evergren, E., McMahon, H.T., and Kozlov, M.M. (2012). Membrane fission is promoted by insertion of amphipathic helices and is restricted by crescent BAR domains. Cell 149, 124–136.

Bricogne, G., Vonrhein, C., Flensburg, C., Schiltz, M., and Paciorek, W. (2003). Generation, representation and flow of phase information in structure determination: recent developments in and around SHARP 2.0. Acta Crystallogr. D Biol. Crystallogr. 59, 2023–2030.

Campelo, F., McMahon, H.T., and Kozlov, M.M. (2008). The hydrophobic insertion mechanism of membrane curvature generation by proteins. Biophys. J. 95, 2325–2339.

Caplan, S., Naslavsky, N., Hartnell, L.M., Lodge, R., Polishchuk, R.S., Donaldson, J.G., and Bonifacino, J.S. (2002). A tubular EHD1-containing compartment involved in the recycling of major histocompatibility complex class I molecules to the plasma membrane. EMBO J. 21, 2557–2567.

Chiang, Y.W., Borbat, P.P., and Freed, J.H. (2005). The determination of pair distance distributions by pulsed ESR using Tikhonov regularization. J. Magn. Reson. 172, 279–295.

Danino, D., Moon, K.H., and Hinshaw, J.E. (2004). Rapid constriction of lipid bilayers by the mechanochemical enzyme dynamin. J. Struct. Biol. 147, 259–267.

Daumke, O., Lundmark, R., Vallis, Y., Martens, S., Butler, P.J., and McMahon, H.T. (2007). Architectural and mechanistic insights into an EHD ATPase involved in membrane remodelling. Nature 449, 923–927.

de Beer, T., Carter, R.E., Lobel-Rice, K.E., Sorkin, A., and Overduin, M. (1998). Structure and Asn-Pro-Phe binding pocket of the Eps15 homology domain. Science 281, 1357–1360.

Emsley, P., Lohkamp, B., Scott, W.G., and Cowtan, K. (2010). Features and development of Coot. Acta Crystallogr. D Biol. Crystallogr. 66, 486–501.

Faelber, K., Posor, Y., Gao, S., Held, M., Roske, Y., Schulze, D., Haucke, V., Noé, F., and Daumke, O. (2011). Crystal structure of nucleotide-free dynamin. Nature 477, 556–560.

Frost, A., Perera, R., Roux, A., Spasov, K., Destaing, O., Egelman, E.H., De Camilli, P., and Unger, V.M. (2008). Structural basis of membrane invagination by F-BAR domains. Cell 132, 807–817.

Gallop, J.L., Jao, C.C., Kent, H.M., Butler, P.J., Evans, P.R., Langen, R., and McMahon, H.T. (2006). Mechanism of endophilin N-BAR domain-mediated membrane curvature. EMBO J. 25, 2898–2910.

Grant, B., Zhang, Y., Paupard, M.C., Lin, S.X., Hall, D.H., and Hirsh, D. (2001). Evidence that RME-1, a conserved C. elegans EH-domain protein, functions in endocytic recycling. Nat. Cell Biol. 3, 573–579.

Hatmal, M.M., Li, Y., Hegde, B.G., Hegde, P.B., Jao, C.C., Langen, R., and Haworth, I.S. (2012). Computer modeling of nitroxide spin labels on proteins. Biopolymers 97, 35–44.

Hohn, M., Tang, G., Goodyear, G., Baldwin, P.R., Huang, Z., Penczek, P.A., Yang, C., Glaeser, R.M., Adams, P.D., and Ludtke, S.J. (2007). SPARX, a new environment for Cryo-EM image processing. J. Struct. Biol. 157, 47–55.

Isas, J.M., Langen, R., Haigler, H.T., and Hubbell, W.L. (2002). Structure and dynamics of a helical hairpin and loop region in annexin 12: a site-directed spin labeling study. Biochemistry 41, 1464–1473.

Jao, C.C., Hegde, B.G., Gallop, J.L., Hegde, P.B., McMahon, H.T., Haworth, I.S., and Langen, R. (2010). Roles of amphipathic helices and the bin/amphiphysin/rvs (BAR) domain of endophilin in membrane curvature generation. J. Biol. Chem. 285, 20164–20170.

Jeschke, G., and Polyhach, Y. (2007). Distance measurements on spin-labelled biomacromolecules by pulsed electron paramagnetic resonance. Phys. Chem. Chem. Phys. 9, 1895–1910.

Kabsch, W. (2010). XDS. Acta Crystallogr. D Biol. Crystallogr. 66, 125–132.

Krauss, M., Jia, J.Y., Roux, A., Beck, R., Wieland, F.T., De Camilli, P., and Haucke, V. (2008). Arf1-GTP-induced tubule formation suggests a function of Arf family proteins in curvature acquisition at sites of vesicle budding. J. Biol. Chem. 283, 27717–27723.

Lai, C.L., Jao, C.C., Lyman, E., Gallop, J.L., Peter, B.J., McMahon, H.T., Langen, R., and Voth, G.A. (2012). Membrane binding and self-association of the epsin N-terminal homology domain. J. Mol. Biol. 423, 800–817.

Larkin, M.A., Blackshields, G., Brown, N.P., Chenna, R., McGettigan, P.A., McWilliam, H., Valentin, F., Wallace, I.M., Wilm, A., Lopez, R., et al. (2007). Clustal W and Clustal X version 2.0. Bioinformatics 23, 2947–2948.

Lasiecka, Z.M., Yap, C.C., Caplan, S., and Winckler, B. (2010). Neuronal early endosomes require EHD1 for L1/NgCAM trafficking. J. Neurosci. 30, 16485–16497.

Lee, D.W., Zhao, X., Scarselletta, S., Schweinsberg, P.J., Eisenberg, E., Grant, B.D., and Greene, L.E. (2005a). ATP binding regulates oligomerization and endosome association of RME-1 family proteins. J. Biol. Chem. 280, 17213–17220.

Lee, M.C.S., Orci, L., Hamamoto, S., Futai, E., Ravazzola, M., and Schekman, R. (2005b). Sar1p N-terminal helix initiates membrane curvature and completes the fission of a COPII vesicle. Cell 122, 605–617.

Lin, S.X., Grant, B., Hirsh, D., and Maxfield, F.R. (2001). Rme-1 regulates the distribution and function of the endocytic recycling compartment in mammalian cells. Nat. Cell Biol. 3, 567–572.

Liu, T.Y., Bian, X., Sun, S., Hu, X., Klemm, R.W., Prinz, W.A., Rapoport, T.A., and Hu, J. (2012). Lipid interaction of the C terminus and association of the transmembrane segments facilitate atlastin-mediated homotypic endoplasmic reticulum fusion. Proc. Natl. Acad. Sci. USA 109, E2146–E2154.

Low, H.H., Sachse, C., Amos, L.A., and Löwe, J. (2009). Structure of a bacterial dynamin-like protein lipid tube provides a mechanism for assembly and membrane curving. Cell 139, 1342–1352.

Ludwig, A., Howard, G., Mendoza-Topaz, C., Deerinck, T., Mackey, M., Sandin, S., Ellisman, M.H., and Nichols, B.J. (2013). Molecular composition and ultrastructure of the caveolar coat complex. PLoS Biol. 11, e1001640.

Lundmark, R., Doherty, G.J., Vallis, Y., Peter, B.J., and McMahon, H.T. (2008). Arf family GTP loading is activated by, and generates, positive membrane curvature. Biochem. J. 414, 189–194.

Mim, C., Cui, H., Gawronski-Salerno, J.A., Frost, A., Lyman, E., Voth, G.A., and Unger, V.M. (2012). Structural basis of membrane bending by the N-BAR protein endophilin. Cell 149, 137–145.

Mizuno, N., Jao, C.C., Langen, R., and Steven, A.C. (2010). Multiple modes of endophilin-mediated conversion of lipid vesicles into coated tubes: implications for synaptic endocytosis. J. Biol. Chem. 285, 23351–23358.

Morén, B., Shah, C., Howes, M.T., Schieber, N.L., McMahon, H.T., Parton, R.G., Daumke, O., and Lundmark, R. (2012). EHD2 regulates caveolar dynamics via ATP-driven targeting and oligomerization. Mol. Biol. Cell 23, 1316–1329.

Murshudov, G.N., Skubák, P., Lebedev, A.A., Pannu, N.S., Steiner, R.A., Nicholls, R.A., Winn, M.D., Long, F., and Vagin, A.A. (2011). REFMAC5 for the refinement of macromolecular crystal structures. Acta Crystallogr. D Biol. Crystallogr. 67, 355–367.

Naslavsky, N., and Caplan, S. (2011). EHD proteins: key conductors of endocytic transport. Trends Cell Biol. 21, 122–131.

Naslavsky, N., Rahajeng, J., Sharma, M., Jovic, M., and Caplan, S. (2006). Interactions between EHD proteins and Rab11-FIP2: a role for EHD3 in early endosomal transport. Mol. Biol. Cell *17*, 163–177.

Oh, K.J., Singh, P., Lee, K., Foss, K., Lee, S., Park, M., Lee, S., Aluvila, S., Park, M., Singh, P., et al. (2010). Conformational changes in BAK, a pore-forming proapoptotic Bcl-2 family member, upon membrane insertion and direct evidence for the existence of BH3-BH3 contact interface in BAK homo-oligomers. J. Biol. Chem. *285*, 28924–28937.

Pannier, M., Veit, S., Godt, A., Jeschke, G., and Spiess, H.W. (2000). Dead-time free measurement of dipole-dipole interactions between electron spins. J. Magn. Reson. *142*, 331–340.

Pant, S., Sharma, M., Patel, K., Caplan, S., Carr, C.M., and Grant, B.D. (2009). AMPH-1/Amphiphysin/Bin1 functions with RME-1/Ehd1 in endocytic recycling. Nat. Cell Biol. *11*, 1399–1410.

Parton, R.G., and del Pozo, M.A. (2013). Caveolae as plasma membrane sensors, protectors and organizers. Nat. Rev. Mol. Cell Biol. *14*, 98–112.

Praefcke, G.J.K., and McMahon, H.T. (2004). The dynamin superfamily: universal membrane tubulation and fission molecules? Nat. Rev. Mol. Cell Biol. *5*, 133–147.

Pucadyil, T.J., and Schmid, S.L. (2009). Conserved functions of membrane active GTPases in coated vesicle formation. Science *325*, 1217–1220.

Schwefel, D., Fröhlich, C., Eichhorst, J., Wiesner, B., Behlke, J., Aravind, L., and Daumke, O. (2010). Structural basis of oligomerization in septin-like GTPase of immunity-associated protein 2 (GIMAP2). Proc. Natl. Acad. Sci. USA *107*, 20299–20304.

Shao, Y., Akmentin, W., Toledo-Aral, J.J., Rosenbaum, J., Valdez, G., Cabot, J.B., Hilbush, B.S., and Halegoua, S. (2002). Pincher, a pinocytic chaperone for nerve growth factor/TrkA signaling endosomes. J. Cell Biol. *157*, 679–691.

Stoeber, M., Stoeck, I.K., Hänni, C., Bleck, C.K., Balistreri, G., and Helenius, A. (2012). Oligomers of the ATPase EHD2 confine caveolae to the plasma membrane through association with actin. EMBO J. *31*, 2350–2364.

Suloway, C., Pulokas, J., Fellmann, D., Cheng, A., Guerra, F., Quispe, J., Stagg, S., Potter, C.S., and Carragher, B. (2005). Automated molecular microscopy: the new Leginon system. J. Struct. Biol. *151*, 41–60.

Tang, G., Peng, L., Baldwin, P.R., Mann, D.S., Jiang, W., Rees, I., and Ludtke, S.J. (2007). EMAN2: an extensible image processing suite for electron microscopy. J. Struct. Biol. *157*, 38–46.

von der Malsburg, A., Abutbul-Ionita, I., Haller, O., Kochs, G., and Danino, D. (2011). Stalk domain of the dynamin-like MxA GTPase protein mediates membrane binding and liposome tubulation via the unstructured L4 loop. J. Biol. Chem. *286*, 37858–37865.

Wang, Q., Navarro, M.V.A.S., Peng, G., Molinelli, E., Goh, S.L., Judson, B.L., Rajashankar, K.R., and Sondermann, H. (2009). Molecular mechanism of membrane constriction and tubulation mediated by the F-BAR protein Pacsin/Syndapin. Proc. Natl. Acad. Sci. USA *106*, 12700–12705.